

 Open access • Proceedings Article • DOI:10.1109/IGARSS.2011.6049491

A post nonlinear mixing model for hyperspectral images unmixing — [Source link](#)

Yoann Altmann, Abderrahim Halimi, Nicolas Dobigeon, Jean-Yves Tourneret

Institutions: University of Toulouse

Published on: 24 Jul 2011 - International Geoscience and Remote Sensing Symposium

Topics: Hyperspectral imaging

Related papers:

- [Supervised Nonlinear Spectral Unmixing Using a Postnonlinear Mixing Model for Hyperspectral Imagery](#)
- [Supervised nonlinear spectral unmixing using a polynomial post nonlinear model for hyperspectral imagery](#)
- [Bayesian unsupervised unmixing of hyperspectral images using a post-nonlinear model](#)
- [Nonlinear spectral unmixing of hyperspectral images using residual component analysis](#)
- [Nonlinear Spectral Unmixing of Hyperspectral Images Using Gaussian Processes](#)

Share this paper:    

View more about this paper here: <https://typeset.io/papers/a-post-nonlinear-mixing-model-for-hyperspectral-images-30h4rg13o0>

A POST NONLINEAR MIXING MODEL FOR HYPERSPECTRAL IMAGES UNMIXING

Yoann Altmann, Abderrahim Halimi, Nicolas Dobigeon and Jean-Yves Tourneret

University of Toulouse, IRIT-ENSEEIH, France

{yoann.altmann,abderrahim.halimi,nicolas.dobigeon,jean-yves.tourneret}@enseeiht.fr

ABSTRACT

This paper studies estimation algorithms for nonlinear hyperspectral image unmixing. The proposed unmixing model assumes that the pixel reflectances are polynomial functions of linear mixtures of pure spectral components contaminated by an additive white Gaussian noise. A hierarchical Bayesian algorithm and an optimization method are proposed for solving the resulting unmixing problem. The parameters involved in the proposed model satisfy constraints that are naturally included in the estimation procedure. The performance of the unmixing strategies is evaluated thanks to simulations conducted on synthetic and real data.

Index Terms— Post nonlinear mixing model, hyperspectral images, MCMC methods, Taylor approximation.

1. INTRODUCTION

Spectral unmixing (SU) is one of the major issues when analyzing hyperspectral images. SU consists of identifying the macroscopic materials present in an hyperspectral image and quantifying the proportions of these materials in all pixels of the image. Most SU strategies assume that pixel reflectances are linear combinations of pure component spectra (endmembers). The resulting linear mixing model (LMM) has been widely used in the literature and has shown promising results. However, as explained in [1], the LMM can be inappropriate for some hyperspectral images, such as those containing sand, trees or vegetation areas [2, 3]. Nonlinear mixing models provide an interesting alternative to overcome the inherent limitations of the LMM. Nonlinear models proposed in the hyperspectral image literature include the bidirectional reflectance-based model proposed by Hapke [4] and the the bilinear models recently studied in [2, 3, 5, 6]. This paper considers a wide class of nonlinear mixing models referred to as *post nonlinear mixing models* (PNMMs). PNMMs are flexible generalizations of the LMM that have been introduced in [7] for source separation problems (see also [8]). In the hyperspectral imagery context, the endmember spectra can be identified as the *sources* whereas the abundances are the *mixing coefficients* involved in the PNMM. This paper addresses the problem of supervised nonlinear SU of hyperspectral images using PNMMs. Supervised unmixing means here that the endmembers (the *sources*) are known, whereas the abundances (the *mixing coefficients*) are unknown and have to be estimated.

Prior knowledge regarding the pure spectral components contained in the observed scene is rarely available in practical applications. As a consequence, the endmember spectra have to be extracted directly from the data using an endmember extraction algorithm (EEA). In the last decades, many EEAs have been studied in

the literature (the reader is invited to consult [9] for a recent review of these methods). Most of existing EEAs implicitly rely on the LMM and might be inappropriate for nonlinear models such as PNMMs. However, as noticed in [1], geometric EEAs are still adapted to identify endmembers and can be reasonably employed when the mixing model involves nonlinearities. Therefore, this paper proposes to extract the endmembers contained in the hyperspectral image using the *vertex component analysis* (VCA) [10]. Once the endmembers have been extracted from the image, we propose to estimate the abundances and the nonlinearity parameters involved in the PNMM using two estimation algorithms based on Bayesian and least-squares (LS) methods.

The paper is organized as follows. Section 2 presents the proposed PNMM for hyperspectral image analysis. Section 3 studies two algorithms for unmixing hyperspectral images using the PNMM. Some simulation results on synthetic and real data are shown and discussed in Section 4. Conclusions are reported in Section 5.

2. POLYNOMIAL POST NONLINEAR MIXING MODEL

This section defines the nonlinear mixing model used for hyperspectral image SU. A PNMM is introduced involving linear and quadratic functions of the abundances. More precisely, the L -spectrum $\mathbf{y} = [y_1, \dots, y_L]^T$ of a mixed pixel is defined as a nonlinear transformation \mathbf{g} of a linear mixture of R spectra \mathbf{m}_r contaminated by additive noise

$$\mathbf{y} = \mathbf{g} \left(\sum_{r=1}^R a_r \mathbf{m}_r \right) + \mathbf{n} = \mathbf{g}(\mathbf{M}\mathbf{a}) + \mathbf{n} \quad (1)$$

where $\mathbf{m}_r = [m_{r,1}, \dots, m_{r,L}]^T$ is the spectrum of the r th material present in the scene, a_r is its corresponding proportion, R is the number of endmembers contained in the image and \mathbf{g} is an appropriate nonlinear function from $(0, 1)^L$ to \mathbb{R}^L . Moreover, L is the number of spectral bands and \mathbf{n} is an additive independent and identically distributed (i.i.d) zero-mean Gaussian noise sequence with variance σ^2 , denoted as $\mathbf{n} \sim \mathcal{N}(\mathbf{0}_L, \sigma^2 \mathbf{I}_L)$, where \mathbf{I}_L is the $L \times L$ identity matrix. Note that the usual matrix and vector notations $\mathbf{M} = [\mathbf{m}_1, \dots, \mathbf{m}_R]$ and $\mathbf{a} = [a_1, \dots, a_R]^T$ have been used in the right hand side of (1).

The choice of the nonlinearity \mathbf{g} deserves a specific attention. Polynomials, sigmoidal functions and combinations of polynomial and sigmoidal nonlinearities have shown interesting properties for source separation [8]. This study focuses on second order polynomial nonlinearities \mathbf{g} defined by

$$\begin{aligned} \mathbf{g}_b : (0, 1)^L &\rightarrow \mathbb{R}^L \\ \mathbf{s} &\mapsto [g_{b,1}(s_1), \dots, g_{b,L}(s_L)]^T \end{aligned}$$

Part of this work has been supported by Direction Generale de l'Armement, French Ministry of Defence.

with $\mathbf{s} = [s_1, \dots, s_L]^T$ and

$$\begin{aligned} g_{b,i} : (0, 1) &\rightarrow \mathbb{R} \\ s_i &\mapsto g_{b,i}(s_i) = s_i + bs_i^2 \end{aligned} \quad (2)$$

for $i = 1, \dots, L$. This particular choice has the advantage of defining the nonlinearity by a unique parameter b whose value allows the importance of the nonlinear terms to be characterized. An interesting property of the resulting nonlinear model referred to as polynomial post nonlinear mixing model (PPNMM) is that it reduces to the classical LMM for $b = 0$. Thus, we can expect unmixing results at least as good as those presented in [11] or [12] for supervised SU. Another motivation for using the PPNMM is the Weierstrass approximation theorem which states that every continuous function defined on an interval can be uniformly approximated by a polynomial with any desired precision [13, p. 15]. As explained in [3], it is reasonable to consider polynomials with first and second order terms (since higher order terms can generally be neglected) which leads to (2). Straightforward computations allow the PPNMM observation vector (for a given pixel of the image) to be expressed as follows

$$\mathbf{y} = \mathbf{M}\mathbf{a} + b(\mathbf{M}\mathbf{a}) \odot (\mathbf{M}\mathbf{a}) + \mathbf{n} \quad (3)$$

where \odot denotes the Hadamard (termwise) product. Note that the resulting PPNMM includes bilinear terms such as those considered in [5].

By studying the derivative of $g_{b,i}$, it is straightforward to show that the nonlinearity parameter b must be lower bounded by $b_{\min} = -0.5$ to make g_b invertible. In this paper, we will assume that b belongs to a bounded interval $(-0.3, 0.3)$ to ensure model invertibility. Moreover, due to physical considerations, the abundance vector \mathbf{a} satisfy the following positivity and sum-to-one constraints

$$\sum_{r=1}^R a_r = 1, \quad a_r \geq 0, \forall r \in \{1, \dots, R\}. \quad (4)$$

3. ESTIMATION METHODS

This section studies two estimation methods that can be used for estimating the parameters \mathbf{a} and b of the proposed PPNMM.

3.1. Hierarchical Bayesian algorithm

The Bayesian estimation algorithm introduced in [14] can be used to estimate the unknown parameters $\boldsymbol{x} = (\mathbf{a}^T, b, \sigma^2)$ of the model (3). Appropriate prior distributions are assigned to the unknown parameters associated to the PPNMM. The posterior distribution of the unknown parameter vector can be derived from

$$f(\boldsymbol{x}|\mathbf{y}) \propto f(\mathbf{y}|\boldsymbol{x})f(\boldsymbol{x}) \quad (5)$$

where \propto means ‘‘proportional to’’, $f(\mathbf{y}|\boldsymbol{x})$ is the likelihood function of the observation vector \mathbf{y} and $f(\boldsymbol{x})$ is the prior distribution of the unknown parameters. As in [14], $f(\boldsymbol{x})$ is set to satisfy all constraints regarding the parameters, i.e., the positivity and sum-to-one constraints for the abundance vector and the inequality constraint for b . The standard Bayesian estimators (minimum mean square error (MMSE) or maximum a posteriori (MAP)) of the PPNMM parameters are then computed from the posterior distribution (5). To alleviate the problems associated with this computation, a Markov chain Monte Carlo method initially studied in [14] can be used. More precisely, an appropriate Gibbs sampler can be used to generate N_{MC}

samples $\boldsymbol{x}^{(1)}, \dots, \boldsymbol{x}^{(N_{MC})}$ asymptotically distributed according to (5). The MAP and MMSE estimators can then be determined by

$$\begin{aligned} \hat{\boldsymbol{x}}_{\text{MMSE}} &= \frac{1}{N_r} \sum_{i=1}^{N_r} \boldsymbol{x}^{(i+N_{\text{bi}})} \\ \hat{\boldsymbol{x}}_{\text{MAP}} &= \arg \max_{\boldsymbol{x}^{(i)}} f(\boldsymbol{x}|\mathbf{y}) \quad i = N_{\text{bi}} + 1, \dots, N_{\text{bi}} + N_r \end{aligned}$$

where N_{bi} is the number of burn-in iterations and $N_r = N_{MC} - N_{\text{bi}}$ is the number of iterations after convergence of the Gibbs sampler. The advantage of this method is its ability to provide point estimates (MAP or MMSE) for the unknown parameters as well as measures of uncertainties (such as confidence intervals) about these estimates. However, it suffers from high computational cost. The next section presents a new estimation strategy which allows this computational cost to be significantly reduced.

3.2. Taylor approximation

An alternative to the Bayesian algorithm presented in section 3.1 is a least-squares (LS) method which has been used successfully for linear unmixing [12]. The LS method associated with (3) consists of minimizing the LS criterion

$$\mathbf{J}(\mathbf{a}, b) = \|\mathbf{y} - \mathbf{g}_b(\mathbf{M}\mathbf{a})\|_2^2 \quad (6)$$

where $\|\cdot\|_2$ is the standard ℓ_2 norm, subject to the following constraints

$$\begin{aligned} \sum_{r=1}^R a_r &= 1, \quad a_r \geq 0, \forall r \in \{1, \dots, R\} \\ b &\geq -0.5. \end{aligned} \quad (7)$$

This minimization of (6) subject to the constraints (7) is not easy to handle.

Following the strategy adopted in [5], we propose to approximate the nonlinearity g_b using a Taylor series expansion where only first-order terms are considered. Let $\boldsymbol{\theta}^{(i)} = [\mathbf{a}^{(i)}, k^{(i)}]^T$ denote the parameter vector estimate at the i th step of the proposed iterative algorithm, where $k^{(i)} = b^{(i)} + 0.5$. Note that the proposed reparametrization ensures all coordinates of $\boldsymbol{\theta}^{(i)}$ satisfy the non-negativity constraint. These constraints are required to apply the fully constrained least squares (FCLS) algorithm presented at the end of this section. The corresponding estimated spectrum can then be written

$$\mathbf{h}(\boldsymbol{\theta}^{(i)}) = \mathbf{M}\mathbf{a}^{(i)} + (k^{(i)} - 0.5) (\mathbf{M}\mathbf{a}^{(i)}) \odot (\mathbf{M}\mathbf{a}^{(i)}) \quad (8)$$

according to the model (3). The Taylor approximation of \mathbf{h} at $\boldsymbol{\theta}^{(i)}$ is

$$\mathbf{h}(\boldsymbol{\theta}) = \mathbf{h}(\boldsymbol{\theta}^{(i)}) + \nabla \mathbf{h}(\boldsymbol{\theta}^{(i)}) (\boldsymbol{\theta} - \boldsymbol{\theta}^{(i)}) + \boldsymbol{\epsilon} \quad (9)$$

where $\nabla \mathbf{h}(\boldsymbol{\theta}^{(i)})$ is the gradient matrix of $\mathbf{h}(\boldsymbol{\theta}^{(i)})$ of size $L \times (R + 1)$, $\boldsymbol{\epsilon}$ is a residual error vector of size $L \times 1$ and $\boldsymbol{\theta}$ is the unknown parameter vector to be estimated. The vector $\boldsymbol{\theta}^{(i+1)}$ can then be estimated by solving the following constrained LS problem

$$\boldsymbol{\theta}^{(i+1)} = \arg \min_{\boldsymbol{\theta}} \left\| \mathbf{y} - \mathbf{h}(\boldsymbol{\theta}^{(i)}) - \nabla \mathbf{h}(\boldsymbol{\theta}^{(i)}) (\boldsymbol{\theta} - \boldsymbol{\theta}^{(i)}) \right\|^2 \quad (10)$$

subject to the constraints (7). Problem (10) can be solved by modifying the FCLS algorithm introduced in [12]. More precisely, the

FCLS algorithm has been introduced to solve the following optimization problem

$$\min_{\mathbf{a}} \|\mathbf{y} - \mathbf{M}\mathbf{a}\|^2, \quad \text{subject to (4)}. \quad (11)$$

The FCLS algorithm includes the sum-to-one constraint of the abundances as an additional observation equation in the criterion to be minimized. The following optimization problem is then obtained

$$\min_{\mathbf{a}} \left\| \begin{bmatrix} \mathbf{y} \\ \delta \end{bmatrix} - \begin{bmatrix} \mathbf{M} \\ \delta \mathbf{1}_R^T \end{bmatrix} \mathbf{a} \right\|_2^2 \quad (12)$$

subject to the non-negativity constraints for the abundance vector \mathbf{a} , where $\delta \in \mathbb{R}^+$ controls the impact of the sum-to-one constraint and $\mathbf{1}_R \in \mathbb{R}^R$ is a vector of ones (see [12] for more details).

Similarly, to solve (10), the sum-to-one constraint for the abundances is included in an additional observation equation, leading to the following optimization problem

$$\min_{\boldsymbol{\theta}} \left\| \begin{bmatrix} \mathbf{z} \\ \delta \end{bmatrix} - \begin{bmatrix} \tilde{\mathbf{M}} \\ \delta \mathbf{1}_R^T \ 0 \end{bmatrix} \boldsymbol{\theta} \right\|_2^2 \quad (13)$$

subject to the non-negativity constraints for the parameter vector $\boldsymbol{\theta}$, where $\tilde{\mathbf{M}} = \nabla \mathbf{h}(\boldsymbol{\theta}^{(i)})$ is an $L \times (R+1)$ matrix, $\delta \in \mathbb{R}^+$ controls the impact of the sum-to-one constraint and

$$\mathbf{z} = \mathbf{y} - \mathbf{h}(\boldsymbol{\theta}^{(i)}) + \nabla \mathbf{h}(\boldsymbol{\theta}^{(i)}) \boldsymbol{\theta}^{(i)} \in \mathbb{R}^L. \quad (14)$$

The iterative procedure stops at the n th iteration, when $\|\boldsymbol{\theta}^{(n)} - \boldsymbol{\theta}^{(n-1)}\|_2^2 \leq \rho$, where ρ is a given threshold (set to $\rho = 10^{-6}$ in our simulations).

4. SIMULATIONS

4.1. Synthetic data

The performance of the proposed nonlinear SU algorithms has been investigated by unmixing 4 synthetic images of size 50×50 . The $R = 3$ endmembers have been extracted from the spectral libraries provided with the ENVI software (i.e., green grass, olive green paint and galvanized steel metal). The different images denoted as I_1, \dots, I_4 have been generated according to the LMM, the bilinear model of [5] (referred to as FM), the generalized bilinear model (GBM) of [6] and the proposed PPNMM, respectively. For each image, the abundance vectors $\mathbf{a}_p, p = 1, \dots, 2500$, have been randomly generated according to a uniform distribution over the simplex defined by the positivity and sum-to-one constraints (4). The nonlinearity coefficients are uniformly drawn in the set $(0, 1)$ for the GBM. The parameter b defining the PPNMM has been drawn uniformly in the interval $(-0.3, 0.3)$. All images have been corrupted by an additive Gaussian noise of variance $\sigma^2 = 2.8 \times 10^{-3}$, corresponding to a signal-to-noise ratio $\text{SNR} = L^{-1} \sigma^{-2} \|f(\mathbf{M}, \mathbf{a})\|^2 \simeq 15$ dB. The quality of the unmixing procedures is measured by comparing the estimated and actual abundance vectors using the root mean square error

$$\text{RMSE} = \sqrt{\frac{1}{PR} \sum_{p=1}^P \|\hat{\mathbf{a}}_p - \mathbf{a}_p\|^2} \quad (15)$$

where \mathbf{a}_p and $\hat{\mathbf{a}}_p$ are the actual and estimated abundance vectors for the p th pixel of the image, P is the number of image pixels and R is

the number of endmembers extracted from the image. Table 1 shows the RMSEs associated with the images I_1, \dots, I_4 and the considered estimation procedures. These results show that the abundances estimated by the Bayesian algorithm and proposed LS method are similar. However, the LS method has the advantage to provide a much smaller computational cost. The unmixing quality can be also evaluated by using the mean reconstruction error

$$\text{RE} = \sqrt{\frac{1}{P} \sum_{p=1}^P \|\hat{\mathbf{y}}_p - \mathbf{y}_p\|^2} \quad (16)$$

where \mathbf{y}_p is the p th observation vector and $\hat{\mathbf{y}}_p$ its estimate (note that $\hat{\mathbf{y}} = \mathbf{M}\hat{\mathbf{a}} + \hat{b}(\mathbf{M}\hat{\mathbf{a}}) \odot (\mathbf{M}\hat{\mathbf{a}})$ for the PPNMM). Table 1 compares the mean reconstruction errors (REs) obtained using the two proposed unmixing algorithms for the 4 synthetic images. These results show that the two algorithms provide similar REs for all images. Fig. 1 shows the histograms of the estimated nonlinearity parameter b (denoted as \hat{b}) for the four images I_1, \dots, I_4 (from left to right) using the Bayesian algorithm and LS method. The histograms are similar for the two algorithms. Moreover, the shape of these histograms seems to be interesting for detecting the kind of linearity or nonlinearity characterizing the spectral mixing model.

	RMSE ($\times 10^{-2}$)		RE ($\times 10^{-2}$)		Time (s)	
	Bayes.	LS	Bayes.	LS	Bayes.	LS
I_1	2.91	2.92	5.28	5.28	5940	3.6
I_2	3.42	3.42	5.29	5.29	6300	4.3
I_3	3.23	3.23	5.28	5.28	6600	4.1
I_4	2.94	2.93	5.28	5.28	5940	4.3

Table 1. RMSEs, REs and computational cost of I_1, \dots, I_4 .

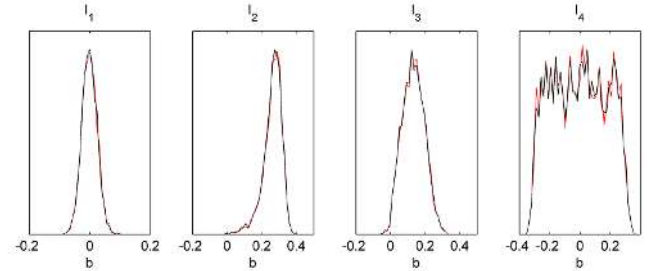


Fig. 1. Distribution of the nonlinearity parameter b estimated by the Bayesian algorithm (red lines) and the LS method (black lines).

4.2. Real data

The real image considered in this section is composed of $L = 189$ spectral bands and was acquired in 1997 by the airborne visible infrared imaging spectrometer (AVIRIS) over the Cuprite mining site in Nevada. A sub-image of size 50×50 pixels has been chosen here to evaluate the proposed unmixing procedure. The scene is mainly composed of muscovite, alunite and kaolinite, as explained in [15]. The endmembers are extracted by VCA [10], with $R = 3$. The estimation algorithms presented in Section 3 have been applied independently to each pixel of the scene using the endmembers extracted by VCA. The abundance maps estimated by the proposed algorithms are presented in Fig. 2. They are similar to the abundance maps that would be obtained with estimation algorithms associated to the

LMM. However, the advantage of the PPNMM is that it allows the nonlinearities between the observations and the endmembers to be estimated. For instance, Fig. 3 (Top) shows the estimated posterior distributions of b on the Cuprite image (2500 pixels). These results show that the observations are nonlinearly related to the endmembers (since $b \neq 0$) but that these nonlinearities are weak (the estimated values of b are close to 0). Fig. 3 (Bottom) also shows the b maps estimated by the two algorithms for the Cuprite scene.

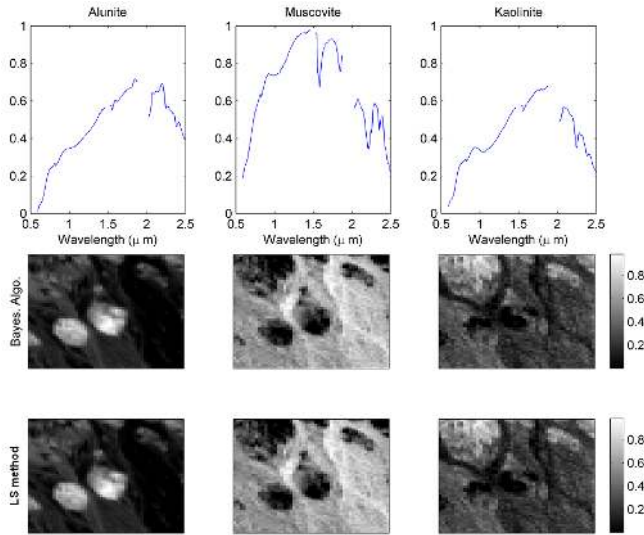


Fig. 2. Top: Spectra estimated by the VCA algorithm for the Cuprite scene. Middle: Abundance maps estimated on the Cuprite scene by the Bayesian algorithm. Bottom: Abundance maps estimated on the Cuprite scene by the LS method.

5. CONCLUSIONS AND FUTURE WORKS

Two nonlinear unmixing algorithms were presented for hyperspectral imagery. These algorithms assumed that the hyperspectral image pixels are related to the endmembers by a polynomial post-nonlinear mixing model. The constraints related to the unknown parameters of this model were considered for the two algorithms. The proposed unmixing strategies provided promising results. Future works include the derivation of nonlinearity detectors based on the proposed model.

6. REFERENCES

- [1] N. Keshava and J. F. Mustard, "Spectral unmixing," *IEEE Signal Processing Magazine*, pp. 44–57, Jan. 2002.
- [2] B. Somers, K. Cools, S. Delalieux, J. Stuckens, D. V. der Zande, W. W. Verstraeten, and P. Coppin, "Nonlinear hyperspectral mixture analysis for tree cover estimates in orchards," *Remote Sensing of Environment*, vol. 113, no. 6, pp. 1183–1193, 2009.
- [3] J. M. P. Nascimento and J. M. Bioucas-Dias, "Nonlinear mixture model for hyperspectral unmixing," in *Proc. SPIE Image and Signal Processing for Remote Sensing XV*, L. Bruzzone, C. Notarnicola, and F. Posa, Eds., vol. 7477, no. 1. SPIE, 2009, p. 74770I.
- [4] B. W. Hapke, "Bidirectional reflectance spectroscopy. I. Theory," *J. Geophys. Res.*, vol. 86, pp. 3039–3054, 1981.
- [5] W. Fan, B. Hu, J. Miller, and M. Li, "Comparative study between a new nonlinear model and common linear model for analysing laboratory

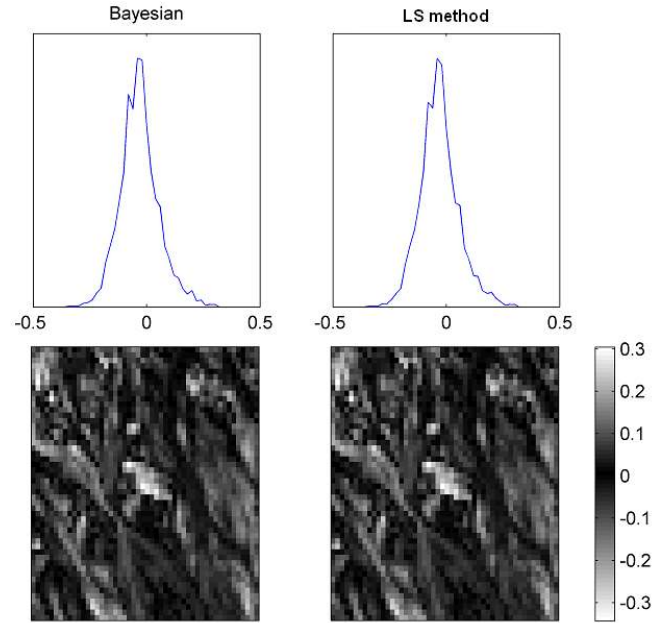


Fig. 3. Top: Estimated distributions of the nonlinearity parameter b . Bottom: Maps of b estimated on the Cuprite scene (left: Bayesian algorithm, right: LS method).

- simulated-forest hyperspectral data," *Remote Sensing of Environment*, vol. 30, no. 11, pp. 2951–2962, June 2009.
- [6] A. Halimi, Y. Altmann, N. Dobigeon, and J.-Y. Tourneret, "Nonlinear unmixing of hyperspectral images using a generalized bilinear model," *IEEE Trans. Geosci. and Remote Sensing*, 2011, to appear.
- [7] C. Jutten and J. Karhunen, "Advances in nonlinear blind source separation," in *Proc. of the 4th Workshop on Independent Component Analysis and Blind Signal Separation (ICA2003)*, Nara, Japan, April 2003, pp. 245–256.
- [8] M. Babaie-Zadeh, C. Jutten, and K. Nayeibi, "Separating convolutive post non-linear mixtures," in *Proc. of the 3rd Workshop on Independent Component Analysis and Signal Separation (ICA2001)*, San Diego, 2001, pp. 138–143.
- [9] M. Parente and A. Plaza, "Survey of geometric and statistical unmixing algorithms for hyperspectral images," in *Proc. IEEE GRSS Workshop on Hyperspectral Image and Signal Processing: Evolution in Remote Sensing (WHISPERS)*, Reykjavik, Iceland, 2010.
- [10] J. M. Nascimento and J. M. Bioucas-Dias, "Vertex component analysis: A fast algorithm to unmix hyperspectral data," *IEEE Trans. Geosci. and Remote Sensing*, vol. 43, no. 4, pp. 898–910, April 2005.
- [11] N. Dobigeon, J.-Y. Tourneret, and C.-I. Chang, "Semi-supervised linear spectral unmixing using a hierarchical Bayesian model for hyperspectral imagery," *IEEE Trans. Signal Process.*, vol. 56, no. 7, pp. 2684–2695, July 2008.
- [12] D. C. Heinz and C.-I. Chang, "Fully constrained least-squares linear spectral analysis method for material quantification in hyperspectral imagery," *IEEE Trans. Geosci. and Remote Sensing*, vol. 29, no. 3, pp. 529–545, March 2001.
- [13] V. J. Mathews and G. L. Sicuranza, *Polynomial Signal Processing*. New York: Wiley, 2000.
- [14] Y. Altmann, A. Halimi, N. Dobigeon, and J.-Y. Tourneret, "Supervised nonlinear spectral unmixing using a polynomial post nonlinear model for hyperspectral imagery," in *Proc. IEEE Int. Conf. Acoust., Speech, and Signal Processing (ICASSP)*, Prague, Czech Republic, 2011.
- [15] N. Dobigeon, S. Moussaoui, M. Coulon, J.-Y. Tourneret, and A. O. Hero, "Joint Bayesian endmember extraction and linear unmixing for hyperspectral imagery," *IEEE Trans. Signal Process.*, vol. 57, no. 11, pp. 2657–2669, Nov. 2009.